Identification of Gip as a novel phage-encoded gyrase inhibitor protein featuring a broad activity profile

Running title: CGP3-encoded Gip inhibits DNA gyrase

Larissa Kever[1], Max Hünnefeld[1], Jannis Brehm[2], Ralf Heermann[2] and Julia Frunzke[1]*

[1]Institute of Bio- und Geosciences, IBG-1: Biotechnology, Forschungszentrum Jülich, 52425 Jülich, Germany

[2]Institut für Molekulare Physiologie, Biozentrum II, Mikrobiologie und Weinforschung, Johannes-Gutenberg-Universität Mainz, 55128 Mainz, Germany

*Corresponding authors:

Julia Frunzke; Email: j.frunzke@fz-juelich.de; Phone: +49 2461 615430

Abstract

Bacteriophages represent a powerful source for the identification of novel antimicrobial proteins. In this study, a screening of small cytoplasmic proteins encoded by the CGP3 prophage of *Corynebacterium glutamicum,* resulted in the identification of the novel gyrase-inhibiting protein Cg1978 (Gip), which shows a direct interaction with the gyrase subunit A (GyrA). In vitro supercoiling assays further suggest a stabilization of the cleavage complex by Gip. Overproduction of Gip in *C. glutamicum* resulted in a severe growth defect as well as an induction of the SOS response. The cells adapted to *gip* overexpression by increasing expression levels of *gyrAB* and by reducing *topA* expression reflecting the homeostatic control of DNA topology. Interestingly, Gip features a similar activity profile towards gyrases of *Escherichia coli, Mycobacterium tuberculosis* and *C. glutamicum.* Therefore, the detailed elucidation of the mechanism of Gip action may provide novel directions for the design of drugs targeting DNA gyrase.

Keywords

Bacteriophages, DNA gyrase, topoisomerase II inhibitors, gyrase inhibitors, prophage induction, *Mycobacterium*

35 **Introduction**

36 Bacteriophages represent the 'dark matter' of the biological world (Hatfull, 2015; Ofir & Sorek,
37 2018; Rohwer & Youle, 2011). With the recent massive expansion in the genomic sequence
38 space, also the number of functionally unknown open reading frames (ORFans) in phage
39 genomes is continuously increasing (Yin & Fischer, 2008). By targeting diverse cellular processes
40 and regulatory hubs in their host cell, bacteriophages represent a rich source for the identification
41 of novel antibacterial proteins as well as for the establishment of highly efficient molecular tools
42 (De Smet et al., 2017; Nobrega et al., 2018; Roach & Donovan, 2015; Schroven et al., 2021).
43 Especially, small cytoplasmic phage proteins have been shown to influence and reprogram a
44 variety of key cellular processes, including transcription, translation, cell division or central
45 metabolism (De Smet et al., 2017; Orr et al., 2020; Storz et al., 2014).

46 The DNA gyrase represents a type IIA topoisomerase present in all bacteria and plays a crucial
47 role in the homeostatic control of DNA topology. Because of its unique ability to introduce negative
48 supercoils into covalently linked double-stranded DNA, gyrase is an essential protein for bacterial
49 cells and a key target of antibacterial agents (Bush et al., 2015). The heterotetrameric enzyme
50 consists of two GyrA and two GyrB subunits ($GyrA_2GyrB_2$). While the GyrA subunit of the enzyme
51 catalyzes the breaking and resealing activity, the GyrB subunit harbors the site of ATP hydrolysis
52 (Reece & Maxwell, 1991; Vanden Broeck et al., 2019). In terms of small molecules, there are
53 currently two major classes of drugs targeting the bacterial gyrase: the aminocoumarins and the
54 quinolones (Bush et al., 2015; Collin et al., 2011). Besides a range of small molecules, also some
55 proteinaceous bacterial toxins were found to inhibit the activity of the gyrase, including microcin
56 B17 (Pierrat & Maxwell, 2003), a glycine-rich peptide found in *E. coli* strains carrying the *mcb*
57 operon, as well as the CcdB toxin as part of the *ccd* toxin-antitoxin system encoded by the F-
58 plasmid (Dao-Thi et al., 2005; Miki et al., 1992).

59 *Corynebacterium glutamicum* – a member of the phylum Actinobacteria – is an important industrial
60 platform organism used for the industrial production of a wide range of value-added compounds,

61 including amino acids, organic acids and proteins (Wendisch et al., 2016). The genome of the
62 model organism *Corynebacterium glutamicum* ATCC 13032 contains four cryptic prophages
63 (CGP1-4) (Frunzke et al., 2008; Ikeda & Nakagawa, 2003). The largest prophage CGP3 (~ 219 kb,
64 including also CGP4) was shown to be inducible in an SOS-dependent as well as in an SOS-
65 independent manner (Helfrich et al., 2015; Nanda et al., 2014; Pfeifer et al., 2016). Recently, the
66 Lsr2-type protein CgpS was identified as a prophage-encoded nucleoid-associated protein
67 involved in the silencing of phage gene expression maintaining the lysogenic state of the large
68 CGP3 prophage (Pfeifer et al., 2016). Interference with CgpS binding was shown to result in
69 prophage activation and consequently cell death.
70 In this study, a systematic screening of small cytoplasmic proteins encoded by the CGP3
71 prophage of *C. glutamicum* resulted in the identification of phage proteins causing severe growth
72 defects and triggering prophage induction. The small phagic protein Cg1978 was further shown
73 to directly target the DNA gyrase enzyme by interacting with the GyrA subunit. Interaction of Gip
74 and GyrA was shown to inhibit the supercoiling activity of the DNA gyrase in vitro. Cg1978 was
75 therefore termed Gip for gyrase inhibiting protein. The function of Gip as a potential phage-
76 encoded gyrase inhibitor is further supported by transcriptome analysis showing the upregulation
77 of *gyrA* and *gyrB* transcripts as a compensatory mechanism to overcome Gip inhibition. Although
78 Gip was shown not to be essential for prophage induction, we hypothesize that Gip plays a role in
79 modulating gyrase activity to enable efficient phage DNA replication.

80 **Results**

81 ***Screening of small CGP3-encoded proteins for an impact on growth and prophage***
82 ***induction***

83 Most of the proteins encoded by the cryptic but still inducible CGP3 prophage are of unknown
84 function. Phage proteins were shown to frequently target key regulatory hubs to shut down
85 bacterial metabolism (Roach & Donovan, 2015). In this study, we screened the impact of overall
86 eleven small (<75 amino acids), cytoplasmic phage-encoded proteins on cellular growth and
87 prophage induction. For this purpose, plasmid-based overexpression (pAN6-*GOI*) of the selected
88 genes of interest was performed in the prophage reporter strain *C. glutamicum* ATCC 13032::P_{lys}-
89 *eyfp.* In previous studies, this genomically integrated reporter (P_{lys}-*eyfp*) was successfully
90 established to translate prophage activation into a fluorescence output (Helfrich et al., 2015).
91 Following this approach, the overproduction of nine out of eleven phage proteins (Cg1902,
92 Cg1910, Cg1924, Cg1925, Cg1971, Cg2026, Cg2035, Cg2045, Cg2046) displayed comparable
93 phenotypes as the empty vector control regarding backscatter signal and fluorescence output
94 measured via flow cytometry (Supplementary Figure S1 A and B). By contrast, overproduction of
95 Cg1914 and Cg1978 showed a significant effect on growth and prophage induction. Cg1914
96 overproduction resulted in a reduced growth rate ($\mu = 0.26 \pm 0.03\ h^{-1}$) and a reduced final
97 backscatter (Figure 1A, *blue line*) compared to the empty vector control pAN6 ($\mu = 0.40 \pm 0.03\ h^{-}$
98 ^{1}). In case of Cg1978, overproduction led to an elongated lag-phase, but the final backscatter as
99 well as the growth rate in the exponential phase ($\mu = 0.38 \pm 0.01\ h^{-1}$) (Figure 1A, *red line*) were
100 comparable to those of the negative control.

101 A comparable impact on cell growth due to cg1914 or cg1978 overexpression was also detected
102 in the prophage-free strain MB001, indicating that the observed growth defect was independent
103 of the presence and/or activity of the CGP3 island (Figure 1B).

104 For both target proteins, Cg1914 and Cg1978, overproduction resulted in an increased
105 fluorescence signal after 24 h cultivation (cg1914: 7.4 ± 2.6 % induced cells, cg1978: 3.5 ± 0.2 %

106 induced cells) indicating CGP3 prophage induction in the respective subpopulation (Figure 1C).
107 As a positive control, we expressed an N-terminally truncated variant of the prophage silencer
108 CgpS (CgpS-N), which was previously shown to trigger prophage induction (Pfeifer et al., 2016).
109 Since overproduction of Cg1914 and Cg1978 showed a high impact on prophage induction, we
110 tested inducibility of the CGP3 prophage in mutants lacking the respective genes using a plasmid-
111 based prophage reporter (P_{lys}-*venus*). Remarkably, the corresponding strains *C. glutamicum*
112 ATCC 13032 Δcg1914 and Δcg1978 featured no difference - neither in cell growth nor in prophage
113 inducibility - upon treatment with the DNA-damaging antibiotic mitomycin C (Tomasz, 1995), which
114 was used to trigger SOS-dependent prophage induction (Supplementary Figure S2). These
115 results indicated that both proteins are not essentially involved in SOS-dependent CGP3
116 induction. Prophage induction, therefore, appeared to be an indirect effect of Cg1914 or Cg1978
117 overproduction. Based on further results described in the following, we focused on the role and
118 cellular target of the small phage protein Cg1978.

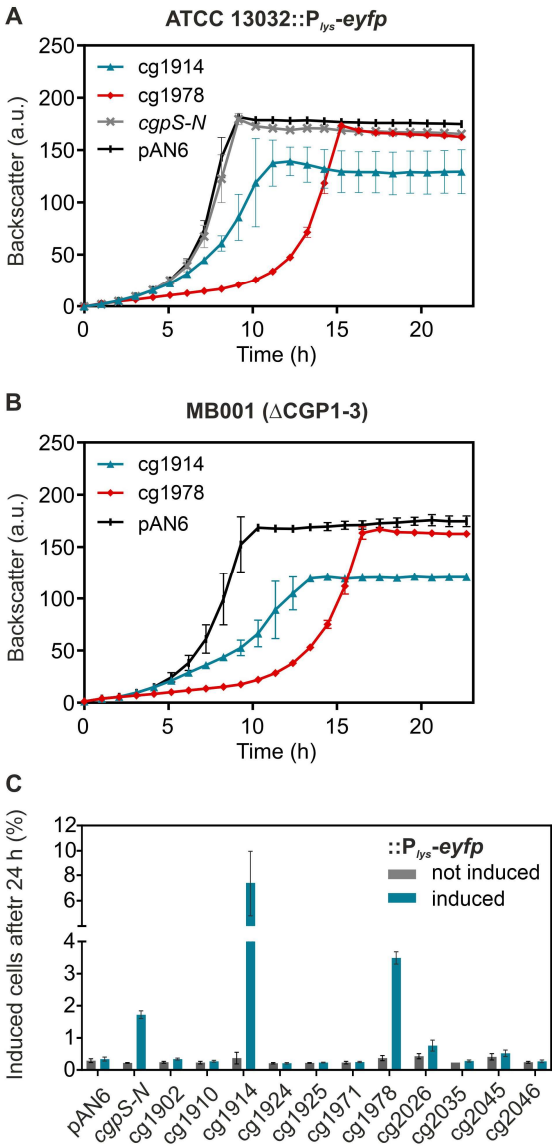

Figure 1: Screening of small phagic proteins regarding their impact on cellular growth and CGP3 induction in *C. glutamicum*. The cultivation of the prophage-reporter strain *C. glutamicum* ATCC 13032::P$_{lys}$-*eyfp* and the prophage-free strain MB001 carrying the corresponding gene sequences of the small proteins on the pAN6 vector (under control of P$_{tac}$) was performed in CGXII-Kan$_{25}$ medium with 2 % (w/v) glucose and 50 µM IPTG for 24 h. All data represent mean values with standard deviations from three independent biological triplicates (n=3). **(A)** Growth curves of the prophage reporter strain (*C. glutamicum* ATCC 13032::P$_{lys}$-*eyfp*) upon small protein overproduction are based on the backscatter measurements in the BioLector® microcultivation system. **(B)** Growth curves of the prophage-free strain MB001 upon small protein overproduction are based on the backscatter measurements in the BioLector® microcultivation system. **(C)**

130 Percentage of induced cells after 24 h cultivation without and with 50 µM IPTG based on the flow
131 cytometric measurements of the prophage reporter strain *C. glutamicum* ATCC 13032::P_{lys}-*eyfp*.
132

133 ***Overproduction of Cg1978 triggers the activation of SOS response and RecA-independent***
134 ***prophage induction***

135 As the CGP3 prophage was already characterized to be inducible in an SOS-dependent as well
136 as in an SOS-independent manner (Helfrich et al., 2015; Nanda et al., 2014; Pfeifer et al., 2016),
137 we determined the SOS-dependency of Cg1978-mediated prophage induction. To this end, the
138 fluorescent outputs of different reporter strains were measured via flow cytometry in a time-
139 resolved manner during cg1978 overexpression. Besides the wildtypic prophage reporter strain
140 ATCC 13032::P_{lys}-*eyfp*, a wildtypic SOS reporter strain ATCC 13032::P_{recA}-*venus* as well as an
141 SOS-deficient prophage reporter strain ATCC 13032 Δ*recA*::P_{lys}-*eyfp* lacking the co-protease
142 RecA – required for the induction of the host SOS response (Janion, 2008) – were used.
143 As described above, overexpression of cg1978 resulted in a similar growth phenotype of all
144 reporter strains characterized by an elongated lag-phase (marked in grey) with subsequent
145 wildtypic growth. The impaired cell growth under cg1978 overexpression conditions was confirmed
146 by microscopy analysis of the prophage reporter strain. Increased levels of Cg1978 led to an
147 elongated cell morphology and a small fraction of cells featuring a strongly increased output of the
148 prophage reporter (Figure 2C, Video S1 and S2).
149 Measurement of the reporter output over time confirmed CGP3 induction, but also revealed an
150 induction of the cellular SOS response (Figure 2B). Interestingly, the wildtypic and the RecA-
151 deficient prophage reporter strain showed nearly the same percentage of induced cells upon
152 cg1978 overexpression throughout the entire measurement, reaching a peak value after 9.5 h of
153 cultivation (Δ*recA*::P_{lys}-*eyfp:* 4.6 ± 0.7, P_{lys}-*eyfp*: 4.8 ± 0.9). These results emphasize CGP3
154 induction as a RecA-independent, indirect effect of cg1978 overexpression.

155 Remarkably, all reporter strains revealed an increasing fluorescence output during the lag-phase,
156 which decreased again upon transition into the exponential growth phase (Figure 2B) suggesting
157 the development of a subpopulation resistant to Cg1978 overproduction effects.

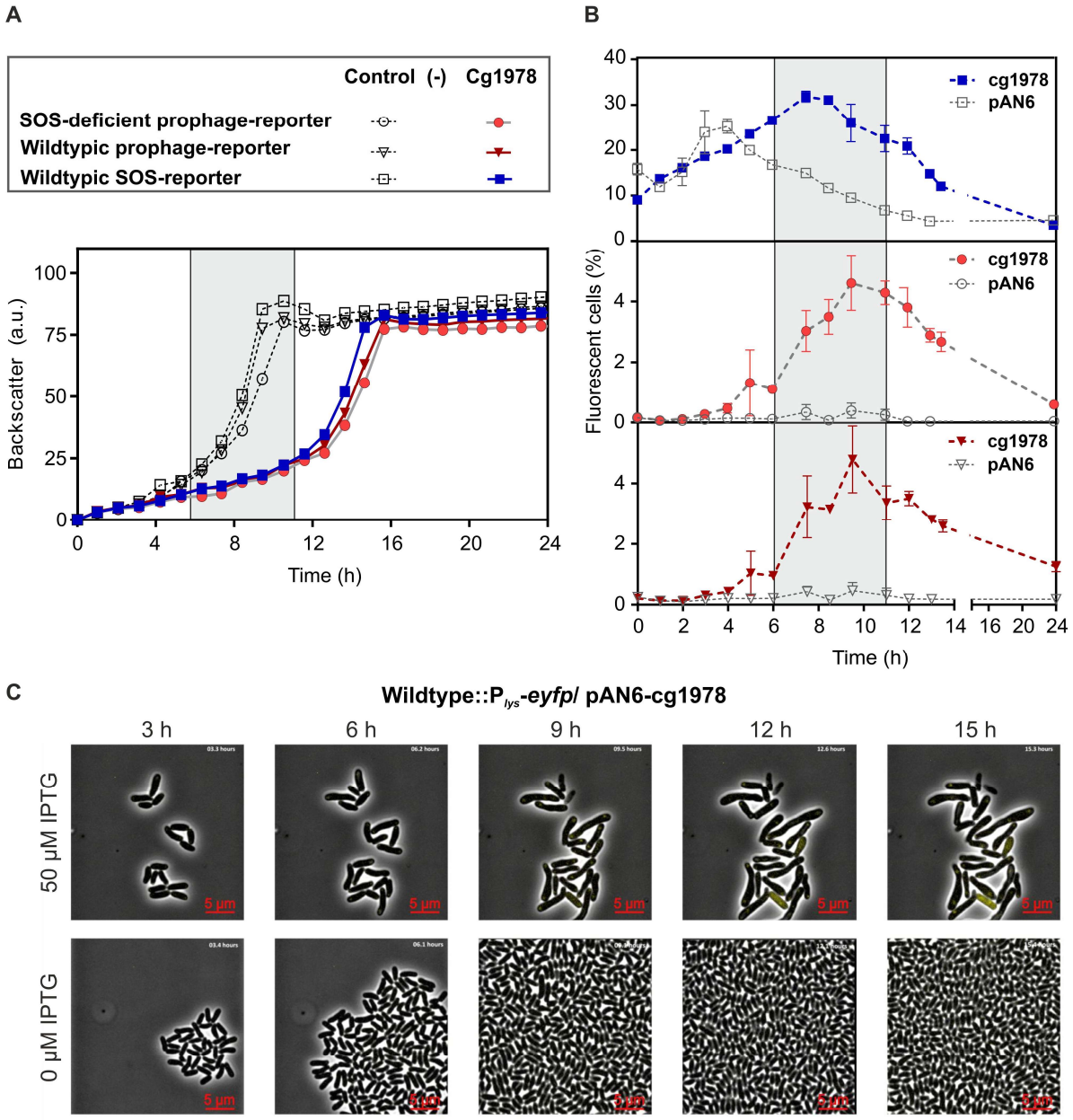

158

159 **Figure 2: Time-resolved measurement of reporter outputs upon Cg1978 overproduction in**
160 ***C. glutamicum* showed an activation of SOS response and RecA-independent prophage**
161 **induction.** Cultivation of a wildtypic SOS reporter strain ATCC 13032::P$_{recA}$-*venus*, a wiltypic
162 prophage reporter strain ATCC 13032::P$_{lys}$-*eyfp* and an SOS-deficient prophage reporter strain

163 ATCC 13032 Δ*recA*::P_{lys}-*eyfp* carrying the plasmids pAN6 or pAN6-cg1978 was performed in the
164 BioLector® microcultivation system in CGXII-Kan_{25} medium with 2 % (w/v) glucose and 50 µM
165 IPTG. All data represent mean values with standard deviations from three independent biological
166 triplicates (n=3). **(A)** Growth curves based on the backscatter measurements in the BioLector®
167 microcultivation system. The elongated lag-phase of the Cg1978 overproducing strain is marked
168 in grey. **(B)** Percentage of induced cells based on the flow cytometric measurements of eYFP or
169 Venus fluorescence of the reporter strains. **(C)** Time-lapse fluorescence microscopy of the
170 *C. glutamicum* prophage reporter strain ATCC 13032::P_{lys}-*eyfp* carrying the pAN6-cg1978
171 plasmid. Cells were grown in PDMS-based microfluidic chip devices using CGXII medium
172 supplemented with 25 µg ml^{-1} kanamycin. The medium was continuously supplied with a flow rate
173 of 300 nl min^{-1} (Grünberger et al., 2015). Overexpression of cg1978 was induced by addition of
174 50 µM IPTG (Video S1 and S2).
175

176 ***Cg1978 directly interacts with gyrase subunit A (GyrA)***

177 To identify the direct cellular target of Cg1978, we performed an in vitro pull-down assay. For this
178 purpose, the small protein Cg1978 containing a C-terminal Strep-tag was overproduced in *E. coli*
179 BL21 (DE3) and purified via affinity purification. The purified target protein was incubated with
180 *C. glutamicum* cell extract and this sample was again passed over a Strep-Tactin column to
181 identify proteins co-purifying with Cg1978. SDS PAGE analysis of proteins co-eluting with Cg1978
182 revealed an additional protein band at ~100 kDa (Figure 3A). Analysis of the co-purified protein
183 via MALDI-TOF as well as analysis of the whole elution fraction via LC-MS/MS indicated the co-
184 purification of Cg1978 with *C. glutamicum (C.g.)* DNA gyrase subunit A (~95 kDa), a subunit of
185 the heterotetrameric ATP-dependent DNA gyrase complex (A_2B_2). This enzyme belongs to the
186 subclass of Type II topoisomerases and plays a key role in DNA metabolism as it is able to
187 introduce negative supercoiling to double-stranded DNA in an ATP-dependent manner (Reece &
188 Maxwell, 1991).
189 As a next step, surface plasmon resonance spectroscopy was used to quantify the interaction
190 between Cg1978 and GyrA by examining binding affinity and kinetics. The sensorgram revealed
191 a stable and specific 1:1 interaction between Cg1978 and GyrA with a high association rate

192 (k_a=9.7x10^4 M^{-1} s^{-1}) and a slow dissociation rate (k_d=9.2 x 10^{-4} s^{-1}) resulting in an overall affinity
193 (K_D) of 5.4 nM (Figure 3B). Purification of Cg1978-C-His and GyrA-N-Strep for SPR analysis are
194 shown in Supplementary Figure S3.

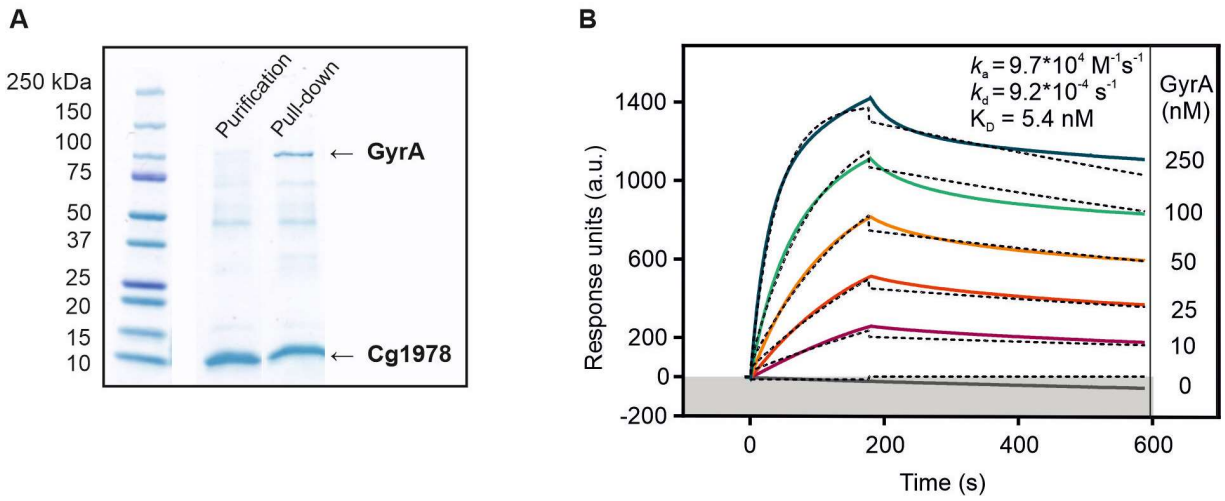

195

196 **Figure 3: Cg1978 directly interacts with the gyrase subunit A (GyrA) in vitro. (A)** The small
197 protein Cg1978 containing a C-terminal Strep-tag was overproduced in *E. coli* BL21 (DE3) and
198 purified via affinity purification. For the pull-down assay the *C. glutamicum* wildtype strain was
199 cultivated in CGXII-Medium with 2 % (w/v) glucose until OD_{600} of 6. The purified target protein was
200 incubated with *C. glutamicum* cell extract and again passed over a Strep-Tactin column aiming at
201 the co-purification of Cg1978 with possible interaction partners. Proteins in the elution fractions
202 were analyzed via SDS-PAGE and further identified using LC-MS/MS and MALDI-TOF. **(B)**
203 Surface plasmon resonance spectroscopy of GyrA binding to Cg1978 (k_a, association constant;
204 k_d, dissociation constant, K_D, equilibrium dissociation constant). The colored lines represent the
205 experimental data, the dotted lines represent the fitted data using 1:1 binding algorithm that were
206 basis for the binding kinetics calculation.
207

208 ***Cg1978 inhibits DNA supercoiling via interaction with DNA gyrase in vitro***

209 Due to its essential role for cell survival, DNA gyrase represents an important drug target of
210 antibiotics and protein-based inhibitors (Collin et al., 2011). Based on the observed growth defect
211 upon Cg1978 overexpression and the interaction with GyrA, we set out to further assess the effect

212 of Cg1978 on gyrase activity by performing in vitro supercoiling inhibition assays with the purified
213 enzyme.
214 For this purpose, Cg1978-C-Strep, GyrA-N-Strep and GyrB-C-Strep from *C. glutamicum* were
215 purified separately using affinity chromatography (Figure 4A). Formation of the heterotetrameric
216 enzyme complex was obtained by incubating equimolar amounts of both gyrase subunits on ice
217 for 30 min. In a first step, the activity of the purified DNA gyrase was measured by incubating
218 0.5 µg relaxed pBR322 plasmid DNA with different gyrase concentrations. Addition of increasing
219 gyrase concentrations led to an increasing supercoiling of the plasmid DNA resulting in a complete
220 supercoiling using 200 nM of *C.g.* gyrase. This concentration was defined as 1 U and was used
221 for testing the potential inhibitory effect of Cg1978 (Figure 4B).
222 As shown in Figure 4C, incubation of increasing concentrations of Cg1978 (0.01-5.0 µM) with 1 U
223 DNA gyrase and relaxed plasmid DNA resulted in a decrease in supercoiling activity of the *C.g.*
224 DNA gyrase. A complete inhibition of the overall supercoiling activity was achieved by addition of
225 5 µM Cg1978. Therefore, we termed the gene product of cg1978 as Gip (gyrase inhibiting protein).
226 To further investigate the activity profile of Gip, we determined its inhibitory activity on the DNA
227 gyrases of *Mycobacterium tuberculosis* and *E. coli.* Gyrase subunits A of the actinobacterial
228 strains *C. glutamicum* and *M. tuberculosis* (*M.tb.*) share a sequence identity of ~71%, while GyrA
229 of *C. glutamicum* and the enterobacterial strain *E. coli* (*E.c.*) only show ~45 % sequence identity
230 (Supplementary Figure S4and S5).
231 As described previously for the DNA gyrase of *C. glutamicum*, 1 U of the *E.c*. and *M.tb.* gyrases
232 were used to examine supercoiling inhibition via Gip. The corresponding gyrase activity assays
233 are shown in Supplementary Figure S6. The supercoiling assay revealed comparable inhibitory
234 concentrations of Gip for the *E.c*. and *M.tb.* gyrase as for the DNA gyrase from *C. glutamicum*.
235 Accordingly, for all tested gyrases 5 µM Cg1978 were successful to achieve a complete inhibition
236 of DNA supercoiling, which results in an accumulation of the linear as well as the relaxed/nicked
237 plasmid conformation (Figure 4C).

238 The inhibition of the *E.c.* gyrase by Gip was further in line with the fact that overexpression of gip
239 resulted in a marked growth defect of *E. coli* in comparison to the empty vector control
240 (Supplementary Figure S7).
241 To exclude, that the inhibitory effect of Gip on the DNA gyrase is caused by any other protein
242 unspecifically co-purified from *E. coli* BL21 (DE3), the total cell extract of this strain was tested
243 regarding its inhibitory effect. No influence on gyrase activity could be observed upon addition of
244 the *E. coli* cell extract. As a positive control, the known fluoroquinolone-based gyrase-inhibitor
245 ciprofloxacin was used and showed a complete inhibition of the supercoiling activity of the *C.g.*
246 gyrase at 50 µM (16.6 µg ml^{-1}). This was in line with already published data for the DNA gyrase of
247 *M. smegmatis*, which showed 50 % inhibition of the supercoiling activity of 1 U gyrase by addition
248 of 10 µg ml^{-1} ciprofloxacin (Manjunatha et al., 2002). In contrast to Gip where we also observed
249 the accumulation of linear plasmid DNA, addition of ciprofloxacin just showed relaxed/nicked
250 plasmid conformation in this assay.

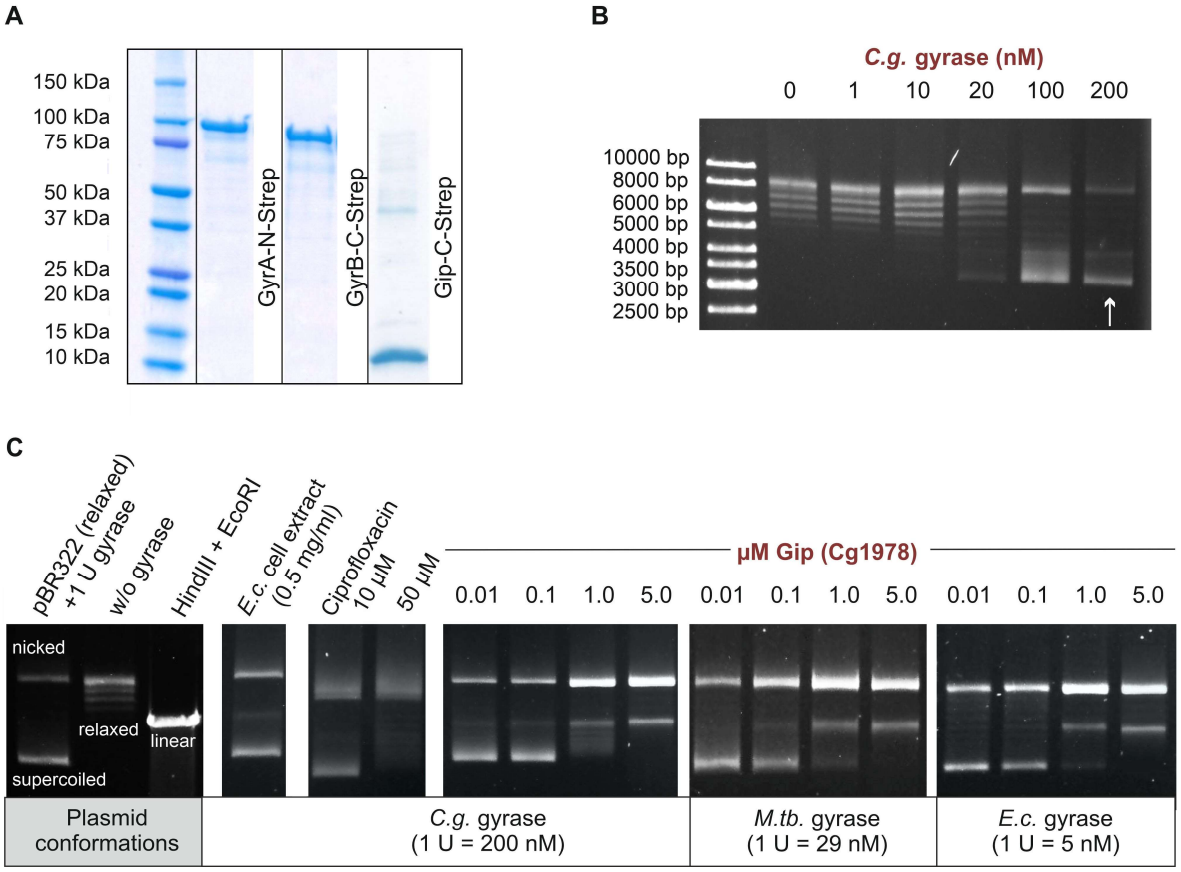

Figure 4: Cg1978 inhibits gyrase supercoiling activity in vitro. The assay was conducted according to the manual of the Gyrase Supercoiling Inhibition Assay-Kit from Inspiralis (Norwich, UK). **(A)** Gyrase subunit A containing a N-terminal and subunit B containing a C-terminal Strep-tag were separately overproduced in *E. coli* BL21 (DE3) and purified via affinity purification. The following gel electrophoresis was performed with 4 -20 % gradient gels at 120 V for 60 min. **(B)** After formation of the heterotetrameric gyrase complex, the activity assay of the purified DNA gyrase from *C. glutamicum* ATCC 13032 was performed to identify the gyrase concentration required for maximal supercoiling of 0.5 µg relaxed plasmid DNA, which was defined as 1 U. **(C)** Supercoiling inhibition assay to test the inhibitory effect of Cg1978 on 1 U of the DNA gyrases from *C. glutamicum* ATCC 13032, *E. coli* and *M. tuberculosis.* The *E. coli* BL21 (DE3) cell extract was further investigated regarding its inhibitory effect as this strain was used for protein overproduction. The known gyrase inhibitor Ciprofloxacin served as a positive control for efficient gyrase inhibition.

265 ***Compensatory expression of* gyrAB *and* topA *as response to gyrase inhibition via Gip***

266 Supercoiling inhibition assays showed that Cg1978 (Gip) is a gyrase-inhibiting protein. As
267 inhibition of the gyrase is lethal for the cell, we wanted to investigate how *gip* overexpression
268 influences genome-wide expression levels. Since the overexpressing strain *gip* revealed a
269 wildtypic growth rate after an elongated lag-phase, we were especially interested to understand
270 how the bacterial host did counteract gyrase inhibition caused by Gip overproduction. To this
271 means, comparative transcriptome analysis of the *C. glutamicum* ATCC 13032 strain containing
272 the empty vector control and the strain containing the overexpression plasmid pAN6-*gip* was
273 performed using DNA microarrays. The shown transcriptomic changes are based on mRNA levels
274 of cells harvested at the same OD_{600} of 6 in the mid-exponential growth phase.

275 The *gip* overexpressing strain showed partially upregulation of CGP3 genes due to
276 overexpression of *gip* (Supplementary Table S1), confirming the prophage induction also revealed
277 by the above described reporter assays. Apart from the CGP3 region, overexpression of *gip* led
278 to upregulation of 352 genes and downregulation of 334 genes reflecting the high impact of gyrase
279 inhibition on overall cell metabolism.

280 Interestingly, both gyrase subunits *gyrA* and *gyrB* were markedly upregulated showing more than
281 4-fold increase in expression levels (Table 1). In contrast, *topA* coding for topoisomerase I, which
282 catalyzes the opposing reaction of the DNA gyrase by removing negative supercoils, showed a
283 reduced expression level. Also expression of further genes involved in DNA metabolism was
284 influenced by *gip* overexpression including exemplarily the downregulation of different genes
285 coding for helicases (cg0838, cg0842, cg0843, cg0845, cg0889 and cg1498). Additionally, nine
286 targets of the SOS key player LexA, e.g. *recN* (DNA repair) and *ftsK* (cell division and chromosome
287 segregation), showed an increased mRNA ratio, which was in line with the high fluorescent outputs
288 of the SOS reporter strain upon Gip overproduction (Table 1). A complete overview on the
289 transcriptomic changes is shown in Supplementary Table S4.

290

291 **Table 1: Impact of *gip* overexpression on global expression levels.** A genome-wide
292 comparison of mRNA levels the *C. glutamicum* ATCC 13032 strain overexpressing *gip* and the
293 wildtype strain carrying the empty vector control was performed. The shown mRNA ratios indicate
294 mean values from three independent biological replicates (n=3). The strains were cultivated in
295 CGXII medium with 2 % (w/v) glucose and 50 µM IPTG and mRNA was prepared from cells at an
296 OD_{600} of 6. The mRNA ratios were calculated by dividing the mRNA levels of *gip* overexpressing
297 strain by the mRNA levels of the strain carrying the empty vector control. The table includes
298 selected genes which showed a changed mRNA level in all experiments (mRNA ratio > 2.0:
299 upregulation (red) or < 0.5: downregulation (green), p-value ≤ 0.05).

Gene locus	Gene name	Annotation	mRNA ratio[a]
		Genes coding for proteins involved in DNA metabolism	
cg0015	*gyrA*	DNA gyrase subunit A, DNA topoisomerase II	6.23
cg0007	*gyrB*	DNA gyrase subunit B, DNA topoisomerase II	4.43
cg0373	*topA*	DNA topoisomerase I	0.40
cg0845		superfamily II DNA/RNA helicase, SNF2 family	0.49
cg0889		putative DNA helicase RecQ	0.48
cg0843		helicase	0.45
cg1498		RecG-like helicase	0.43
cg0842		putative DNA helicase	0.39
cg0838		helicase	0.22
		LexA target genes	
cg1602	*recN*	DNA repair protein	10.96
cg1255		putative HNH endonuclease, conserved	5.11
cg0470	*htaB*	secreted heme transport-associated protein	4.41
cg0738	*dnaE2*	DNA polymerase III subunit α (EC:2.7.7.7)	3.11
cg1288		putative multidrug efflux permease of the major facilitator superfamily	2.83
cg1080		putative multicopper oxidase	2.67
cg2158	*ftsK*	cell division protein	2.46
cg0713		hypothetical protein, conserved	2.13
cg2114	*lexA*	transcriptional regulator, involved in SOS/stress response, LexA-family	2.09
cg2950	*radA*	DNA replication, recombination, repair, and degradation	0.48
cg2381		Unknown function	0.47
cg0834	*tusE*	Carbon source transport and metabolism	0.34
cg0841		Unknown function	0.31
cg1314	*putP*	Amino acid transport and metabolism	0.30
cg3345		Unknown function	0.24

[a] The mRNA ratios were calculated by dividing the mRNA levels of *gip* overexpressing strain by the mRNA levels of the strain carrying the empty vector control.

300 **Discussion**

301 In this study, a screening of small cytoplasmic proteins encoded by the CGP3 prophage of
302 *C. glutamicum* resulted in the identification of Gip (Cg1978, 6.8 kDa) representing a novel gyrase
303 inhibitor protein. Overproduction of Gip resulted in significant growth defects and prophage
304 induction in a subpopulation. Further characterization of this small phagic protein confirmed a
305 specific, stable and high affinity interaction with the GyrA subunit and an inhibition of the
306 supercoiling activity of the DNA gyrase in vitro.

307 The DNA gyrase possesses the unique ability to catalyze the ATP-dependent negative
308 supercoiling of double-stranded DNA by cleaving and rejoining (Bush et al., 2015). Supercoiling
309 inhibition assays showed that Gip-mediated gyrase inhibition resulted in accumulation of the linear
310 plasmid conformation, while no more supercoiled plasmid DNA was detectable (Figure 4). This
311 observation suggests a similar mode of action like synthetic fluoroquinolones and the well-
312 characterized proteinaceous bacterial toxins Microcin B17 (MccB17, 3.1 kDa) and CcdB
313 (11.7 kDa), which poison the DNA gyrase by stabilizing the gyrase-DNA cleavage complex leading
314 to double strand DNA breaks (Bernard et al., 1993; Drlica & Malik, 2003; Pierrat & Maxwell, 2003).
315 In contrast, natural-derived aminocoumarins (e.g. novobiocin) inhibit ATP hydrolysis as the
316 binding site overlaps with the ATP binding pocket of the GyrB subunit (Maxwell & Lawson, 2003).
317 Remarkably, the tested gyrases of *E. coli, M. tuberculosis* and *C. glutamicum* showed a very
318 similar susceptibility to Gip-mediated inhibition. In all cases a complete inhibition of supercoiling
319 was achieved upon addition of 5 µM Gip in in vitro assays. In contrast, the inhibitory activity of
320 CcdB and MccB17 were described to be specific to the DNA gyrase of their bacterial host *E. coli*
321 as the gyrase of *M. smegmatis* was not poisoned by these proteins in vitro (Chatterji et al., 2001).
322 Even though the DNA gyrase is a conserved protein among bacteria, Gram-positive and Gram-
323 negative bacteria show substantial differences in the amino acid sequence of GyrAB
324 (Madhusudan & Nagaraja, 1996; Manjunatha et al., 2000). Accordingly, the absence of specific
325 target residues potentially explains the different levels of susceptibility of the *E. coli* and

326 *M. smegmatis* gyrase to the CcdB and MccB17 toxins (Chatterji et al., 2001). In contrast to this,
327 supercoiling inhibition assays performed in this study suggested that Gip targets a conserved fold
328 in the GyrA subunit. However, further studies and structural analysis are required to elucidate the
329 exact molecular mechanism of Gip-mediated gyrase inhibition.
330 In line with the proposed mode of action, reporter outputs of the RecA-dependent SOS reporter
331 strain and transcriptomic analysis of Gip overproducing cells revealed an induction of the SOS
332 response (Figure 2B, Table 1). This finding conforms to already published data describing an
333 activation of SOS response as one of the pleiotropic effects of gyrase inhibition (Jeong et al.,
334 2006). Stabilization of the gyrase-cleaved DNA complex results in arrested replication forks and
335 widespread DNA damage by stimulating the formation of DNA breaks triggering the SOS response
336 (DeMarini & Lawrence, 1992; Dwyer et al., 2007).
337 Gip overproduction was further shown to activate the induction of the CGP3 prophage. However,
338 the fact that the observed growth defect of Gip overproducing cells is independent of the presence
339 of the CGP3 prophage (Figure 1B) and that deletion of *gip* did not result in an altered inducibility
340 of CGP3 (Figure S2) emphasized prophage activation as an indirect effect of Gip overproduction.
341 Recent studies already confirmed that CGP3 is inducible in an SOS-dependent as well as in an
342 SOS-independent manner (Helfrich et al., 2015; Nanda et al., 2014; Pfeifer et al., 2016). As the
343 wildtypic and the RecA-deficient prophage reporter strain revealed nearly identical fluorescent
344 outputs, we propose that prophage induction occurred mainly in a RecA-independent manner.
345 Here, changes in DNA topology due to gyrase inhibition might be a possible reason for CGP3
346 induction. The lysogenic state of CGP3 is maintained by the Lsr2-type silencer protein CgpS,
347 which was shown to target more than 35 AT-rich regions within the CGP3 element (Pfeifer et al.,
348 2016). The formation of this dense nucleoprotein complex was shown to be crucial for efficient
349 CgpS-mediated silencing (Wiechert et al., 2020). Especially in case of proteins targeting AT-rich
350 DNA sequences, the topological state of DNA can affect protein-DNA interactions (Dorman &
351 Dorman, 2016). Apart from that, different studies already demonstrated an influence of DNA

352 topology on the λ repressor and the lysogenic-lytic decision of phage λ (Ding et al., 2014;
353 Norregaard et al., 2013, 2014).
354 Regarding the native function of Gip, we hypothesize that encoding a gyrase inhibitor could be
355 advantageous for the phage as it might enable a more efficient phage DNA replication by
356 modulating gyrase activity. Similar assumptions were previously reported for the protein 55.2
357 encoded by the T4 phage of *E. coli*. By modulating DNA relaxation activity of TopoI, gp55.2 was
358 proposed to be required for an optimal phage yield during infection (Mattenberger et al., 2015).
359 Global topological alterations caused by Gip overproduction were also reflected by the
360 transcriptome analysis revealing a marked impact on global gene expression patterns (Table 1).
361 Particularly noteworthy in this context are the significantly increased mRNA levels of *gyrA* and
362 *gyrB* as well as the downregulation of *topA*. Since the DNA topology modulatory proteins, gyrase
363 and topoisomerase I (TopoI), catalyze opposing reactions of DNA supercoiling and relaxation, the
364 observed effect likely reflects compensatory mechanisms ensuring DNA topology homeostasis
365 (Massé & Drolet, 1999; Reece & Maxwell, 1991). As the DNA gyrase is indispensable for
366 replication and transcription by changing the topological state of DNA, its inhibition was previously
367 described to globally affect the gene expression profile (Guha et al., 2018; Jeong et al., 2006).
368 Previous studies showed further that expression of the *gyrAB* and *topA* is controlled in a
369 supercoiling-sensitive manner: While increasing DNA relaxation stimulates *gyrAB* expression
370 (Menzel & Gellert, 1983), it represses expression of *topA* allowing a homeostatic maintenance of
371 DNA topology (Ahmed et al., 2016). As gyrase inhibition causes DNA relaxation, increased
372 expression levels of *gyrAB* and decreased expression level of *topA* are a well-known
373 compensatory mechanism of gyrase inhibition (Cheung et al., 2003; Jeong et al., 2006; Menzel &
374 Gellert, 1983). The adaptation at the level of gene expression could then explain the resumed
375 growth of the *gip* expressing strain – reaching almost wildtypic growth rates after a pronounced
376 lag phase (Figure 1).

377 In summary, we have identified Gip as a novel gyrase inhibitor protein encoded by the CGP3
378 prophage of *C. glutamicum.* In vitro experiments provided evidence for a similar mode of action of
379 Gip compared to the bacterial toxin CcdB and microcin B17 by stabilizing the gyrase-DNA
380 cleavage complex via interaction with GyrA – thereby preventing DNA supercoiling. Activity
381 profiling of Gip revealed a broad susceptibility of different gyrases from Gram-positive and Gram-
382 negative bacteria. The mycobacterial DNA gyrase has already been used as a target for anti-
383 mycobacterial therapy and fluoroquinolones show only limited success as second-line drugs due
384 to increasing multidrug-resistance (Falzon et al., 2013). Therefore, a detailed elucidation of the
385 mechanism of action of Gip may permit the design of gyrase inhibitors with a broad activity profile.

386 **Material and methods**

387 ***Bacterial strains and growth conditions***

388 All bacterial strains and plasmids used in this study are listed in Supplementary Table S1 and S2,
389 respectively. *Corynebacterium glutamicum* ATCC 13032 (NCBI reference: NC_003450.3) was
390 used as wild type strain (Ikeda & Nakagawa, 2003). For growth studies and fluorescence
391 measurements as well as for transcriptome analysis, *C. glutamicum* cells were pre-cultivated in
392 BHI (brain heart infusion, Difco BHI, BD, Heidelberg, Germany) at 30 °C and 170 rpm for 8 hours.
393 The pre-culture was used to inoculate an overnight-culture in CGXII minimal medium with 2 %
394 (w/v) glucose, which was cultivated under the same conditions. The next day, the overnight-culture
395 was finally used to inoculate the main culture in CGXII minimal medium with 2 % (w/v) glucose to
396 an OD_{600} of 1. To all media, kanamycin was added in a concentration of 25 µg ml^{-1}. Gene
397 expression was induced using 50 µM IPTG (Isopropyl β-D-1-thiogalactopyranoside). For standard
398 cloning applications, *E. coli* DH5α was cultivated in Lysogeny Broth (Difco LB, BD, Heidelberg,
399 Germany) medium containing 50 µg ml^{-1} kanamycin (LB Kan_{50}) at 37°C and 120 rpm. For protein
400 overproduction and following purification, *E. coli* BL21 (DE3) strain was used. Pre-cultivation was
401 performed in LB Kan_{50} medium, which was incubated overnight at 37 °C and 120 rpm. The main
402 culture in LB Kan_{50} medium was inoculated to an OD_{600} of 0.1 using the pre-culture. At an OD_{600}
403 of 0.6 gene expression was induced using 100 µM IPTG. Cells were harvested after additional
404 24 h incubation at 16 °C.

405

406 ***Recombinant DNA work and cloning techniques***

407 All plasmids and oligonucleotides used in this study are listed in Supplementary Table S2 and S3,
408 respectively. Standard cloning techniques like PCR and restriction digestion were performed
409 according to standard protocols (Sambrook & Russell, 2001). In all cases, Gibson assembly was
410 used for plasmid construction (Gibson, 2011). DNA regions of interest were amplified via PCR
411 using the chromosomal DNA of *C. glutamicum* ATCC 13032 as template. The plasmid backbone

412 was cut using the indicated restriction enzymes. Sequencing and synthesis of oligonucleotides
413 was performed by Eurofins Genomics (Ebersberg, Germany). Genomic deletions were
414 constructed using the pK19*mobsacB* plasmid and the two-step homologues recombination
415 method (Niebisch & Bott, 2001). The 500 bp up- and downstream regions of the respective gene
416 were amplified using the oligonucleotides listed in Supplementary Table S3. Both PCR products
417 and the digested pK19*mobsacB* plasmid (with BamHI, EcoRI) were assembled via Gibson
418 assembly (Gibson, 2011). Correct deletion was verified by sequencing of the colony PCR product
419 with the indicated oligonucleotides (Supplementary Table S3).
420
421 ***Microtiter cultivation and reporter assays***
422 For growth experiments and fluorescence assays, the BioLector® microcultivation system of m2p-
423 labs (Aachen, Germany) was used (Kensy et al., 2009). The main cultivation was executed in
424 FlowerPlates (MTP-48-B, m2p-labs) at 30 °C and 1200 rpm as described in (Heyer et al., 2012)
425 using 750 µl of CGXII-Kan_{25} minimal media with 2% (w/v) glucose containing 50 µM IPTG and
426 25 µg ml^{-1} kanamycin. During cultivation, biomass was measured as a function of backscattered
427 light intensity with an excitation wavelength of 620 nm (filter module: λ_{Ex}/ λ_{Em}: 620 nm/ 620 nm,
428 gain: 15), while fluorescence intensity was recorded with an excitation wavelength of 488 nm and
429 an emission wavelength of 520 nm (filter module: λ_{Ex}/ λ_{Em}: 488 nm/ 520 nm, gain: 60). The
430 measurements of backscatter and fluorescence were taken in 15 min intervals.
431
432 ***Protein purification via affinity tags***
433 For heterologous protein overproduction, *E. coli* BL21 (DE3) cells containing the pET-cg1978-C-
434 *strep* plasmid, the pET-*gyrA*-N-*strep* plasmid, the pET-*gyrB*-C-*strep* plasmid or the pET-cg1978-
435 C-*his* plasmid were cultivated as described in bacterial strains and growth conditions.
436 Cell harvesting and disruption were performed as described by (Pfeifer et al., 2016) using buffer
437 A (100 mM Tris-HCl, pH 8.0) for cell disruption and buffer B (100 mM Tris-HCl, 250 mM NaCl,

438 pH 8.0) for purification. Purification of Strep-tagged Cg1978 was conducted by applying the
439 supernatant to an equilibrated 2 ml Strep-Tactin®-Sepharose® column (IBA, Göttingen,
440 Germany). After washing with 20 ml buffer B, the protein was eluted with 6 ml buffer B containing
441 15 mM d-desthiobiotin (Sigma Aldrich). Purification of GyrA-N-Strep and GyrB-C-Strep were
442 conducted in the same way using an adjusted buffer B_{gyr} for cell disruption and purification (buffer
443 B_{gyr}: 20 mM Tris-HCl, 500 mM NaCl, 10 % (w/v) glycerol, 1 mM DTT, pH 7.9).
444 For purification of Cg1978-C-His, the cell pellet was resuspended in 50 ml TNI buffer (20 mM Tris-
445 HCl, 20 mM imidazole, pH 8.0) and cells were disrupted as described above. Purification of His-
446 tagged Cg1978 was performed by applying the supernatant to an equilibrated 2 ml Ni-NTA column
447 (Invitrogen, Kalifornien, USA). After washing with 30 ml TNI20 buffer, the protein was eluted with
448 increasing imidazole concentrations using TNI buffer (20 mM Tris-HCl, pH 8.0) containing 50 mM,
449 100 mM, 200 mM or 400 mM imidazole.
450 After every purification, the elution fractions with the highest protein concentration were pooled
451 and analyzed with SDS-PAGE (Laemmli, 1970) using a 4–20% Mini-PROTEAN® gradient gel (Bio
452 Rad, Munich, Germany).
453
454 ***In vitro pull-down assay and MALDI-TOF analysis***
455 Protein purification of Cg1978-C-Strep was conducted as described above. The elution fractions
456 showing the highest protein concentration in a Bradford-assay (Bradford, 1976) were pooled and
457 purified with size-exclusion chromatography using PD10 desalting columns (GE Healthcare) and
458 buffer B (100 mM Tris-HCl, 250 mM NaCl, pH 8.0) according to manufacturer´s manual to remove
459 excess desthiobiotin. For the detection of possible interaction partners of the target protein on a
460 protein-protein level, *C. glutamicum* ATCC 13032 wildtype cells were cultivated in BHI medium.
461 At an OD_{600} of 5-6 the cells were harvested at 11.325 *g* and 4 °C for 15 min and cell pellet of
462 100 ml cell culture was resuspended in 25 ml buffer A (100 mM Tris-HCl, pH 8.0) with cOmplete™

463 Proteinase inhibitor (Roche). Cell disruption was performed using the French Press cell with a
464 pressure of 172 mPA for five passages, followed by a centrifugation step at 5000 *g* for 50 min.
465 For co-purification of possible protein interaction partners, the purified target protein Cg1978 was
466 incubated with the *C. glutamicum* crude extract at RT for 1 h. After loading the mixture to the
467 StrepTactin column, the purification was performed as described above.
468 The elution fractions with the highest protein concentration were precipitated by addition of
469 100 % (w/v) trichloroacetic acid (TCA) in a volume ratio of 4 units protein to 1 unit TCA (Sivaraman
470 et al., 1997). After incubation at 4 °C overnight the precipitation approach was centrifuged for
471 5 min at 14.000 g. The supernatant was discarded and the pellet was washed with 200 µl cold
472 acetone twice. Afterwards the pellet was dried for 10 min at 95 °C and resuspended in 30 µl 1.5 x
473 SDS loading buffer for gel electrophoresis or in 30 µl trypsin reaction buffer provided by the Trypsin
474 Singles, Proteomics Grade kit (Sigma-Aldrich) for LC-MS/MS sample preparation.
475 Analysis of elution fractions via SDS-PAGE (Laemmli, 1970) was performed using a 4–20% Mini-
476 PROTEAN® gradient gel (Bio Rad, Munich, Germany). After staining of the gels with Coomassie
477 dye based RAPIDstain solution (G- Biosciences, St. Louis, MO , USA) MALDI-TOF-MS
478 measurements were performed with an Ultraflex III TOF/TOF mass spectrometer (Bruker
479 Daltonics, Bremen, Germany) for identification of the co-purified proteins (Bussmann et al., 2010).
480 Elution fractions were further analyzed via LC-MS/MS.
481
482 ***LC-MS/MS sample preparation and measurement***
483 LC-MS/MS after TCA precipitation was executed using the Trypsin Singles, Proteomics Grade kit
484 (Sigma-Aldrich) according to the manufacturer's instruction. The prepared tryptic peptide samples
485 were separated chromatographically on a nanoLC Eksigent ekspert™ 425 LC system in microLC
486 modus (Sciex) coupled with a 25 Micron ESI Electrode to a TripleTof™ 6600 mass spectrometer
487 (Sciex). As a trap, a YMC-Triart C18 column with the dimension 5 x 0.5 mm ID, 3 µm, 12 nm

488 (YMC) was used, combined with a YMC-Triart C18 column with 150 x 0.3 mm ID, 12 nm, S-3µm
489 (YMC) as analytical column. The column oven was set to 40°C.
490 For trapping, 2% acetonitrile in dd.H_2O with 0.5% formic acid served as a loading solvent, while
491 0.1 % formic acid was used as mobile phase A and acetonitrile with 0.1% formic acid (both LC-
492 MS grade, ROTISOLV®, ≥ 99.9%, Carl Roth) as mobile phase B. First, 10 µl of each sample
493 containing up to 8 µg of digested protein was loaded from the cooled autosampler onto the trap
494 column using 100% loading solvent for 10 minutes at 10 µl min^{-1} for desalting and enrichment.
495 For the following separation of the peptides on the analytical column a linear gradient with
496 increasing concentrations of mobile phase B was used starting with 97 % A and 3 % B and a flow
497 rate of 5 µL min^{-1} as initial condition. During Information Dependent Acquisition (IDA) and SWATH
498 measurements the following source and gas settings were applied: 5500 V spray voltage, 35 psi
499 curtain gas, 12 psi ion source gas 1, 20 psi ion source gas 2, and 150°C interface heater. Each
500 sample was injected three times.
501 For shotgun measurements the mass spectrometer was operated with a “top 50” method: Initially,
502 a 250 ms survey scan (TOF-MS mass range m/z 400-1500, high-resolution mode) was collected
503 from which the top 50 precursor ions were automatically selected for fragmentation, whereby each
504 MS/MS 97 Appendix event (mass range m/z 170-1500, in high sensitivity mode) consisted of a
505 40 ms fragment ion scan. For parent ion selection, the precursor ion intensity served as the main
506 selection criterion. Ions with an intensity exceeding 100 counts per second and with a charge state
507 of 2+ to 5+ were preferentially selected. Selected precursors were added to a dynamic exclusion
508 list for 22 s and subsequently isolated using a quadrupole resolution of 0.7 amu and fragmented
509 in the collision cell with a rolling collision energy (CE) of 10 eV. If less than 50 precursor ions
510 fulfilling the selection criteria were detected per survey scan, the detected precursors were
511 subjected to extended MS/MS accumulation time to maintain a constant total cycle time of 2.3 s.

512 For data analysis the IDA data were processed with ProteinPilot™ (V5.01, Sciex, USA) using the
513 ParagonTM Algorithm for peptide identification and the ProGroup™ Algorithm for protein
514 identification.
515
516 ***DNA microarrays***
517 For a comparative transcriptome analysis of *C. glutamicum* ATCC 13032 carrying the empty pAN6
518 vector and cells carrying the pAN6-cg1978 vector, cultivation was performed as described in
519 'Bacterial strains and growth conditions' using CGXII minimal media with 2% (w/v) glucose and
520 50 µM IPTG. For both strains, cells were harvested at an OD_{600} of 6. RNA purification was done
521 using the „RNeasy Mini"-Kit (QIAGEN) according to the manufacturer´s manual. The preparation
522 of labeled cDNA and DNA microarray analysis was performed as described previously (Donovan
523 et al., 2015). The data processing was executed with an in-house software according to (Polen &
524 Wendisch, 2004). Genes with an mRNA ratio (sample/neg. control) > 2.0 (p-value < 0.05) were
525 classified as upregulated, whereas genes with an mRNA ratio < 0.5 (p-value < 0.05) were
526 classified as downregulated. Array data were deposited in the GEO database
527 (ncbi.nlm.nih.gov/geo) with accession number GSE151224.
528
529 ***Flow cytometry***
530 Analysis of fluorescent reporter outputs at the single cell level was performed using the BD
531 Accuri™ C6 Plus flow cytometer (BD Bioscience, Germany). The chromophore of the yellow
532 fluorescent protein eYFP or Venus was excited with a blue dye laser with an excitation wavelength
533 of 488 nm. Fluorescence emission of eYFP and Venus was measured using a 530/30 nm standard
534 filter. Particle size was detected using the forward light scatter (FSC). The flow cytometer was
535 started up by flushing with filtered, dd. H_2O for 10 min. For preparing flow cytometry samples, cell
536 cultures were mixed with 1 ml flow cytometric fluid (BD™ 342003 FACS-flow Sheath Fluid). The

537 concentration of the samples was adjusted to a measurement of 2.000 to 8.000 events/s. Flow
538 cytometric data were analyzed using FlowJo V10 software (Tree Star, Ashland, OR).
539
540 ***Cultivation and perfusion in microfluidic device***
541 Single-cell analysis of cg1978 overexpressing cells was performed using an in-house developed
542 microfluidic platform (Grünberger et al., 2015; Grünberger et al., 2013; Helfrich et al., 2015).
543 Cultivation and time-lapse imaging was performed in CGXII medium with 2% (w/v) glucose and
544 25 µg ml^{-1} kanamycin as described by (Pfeifer et al., 2016). Overexpression of cg1978 in the
545 prophage reporter strain ATCC 13032::P_{lys}-*eyfp* was induced by adding 50 µM IPTG to the
546 medium. An uninduced control served as a reference.
547
548 ***Supercoiling inhibition assay***
549 For the supercoiling inhibition assay, Cg1978 as well as both gyrase subunits (GyrA and GyrB)
550 were purified by the means of a C-terminal Strep-Tag for Cg1978 and GyrB and an N-terminal
551 Strep-Tag for GyrA as described above. Using PD10 desalting columns (GE Healthcare, Illinois,
552 U.S) the buffer of Cg1978 was exchange to PBS (137 mM NaCl, 2.7 mM KCl, 8 mM Na_2HPO_4,
553 1.5 mM KH_2PO_4, pH 7.4). In case of GyrA and GyrB, the buffer was exchanged to 50 mM Tris-
554 HCl, pH 7.9, 30 % (w/v) glycerol, 5 mM DTT. Formation of the heterotetramic gyrase complex was
555 obtained by incubating equimolar amounts of GyrA and GyrB for 30 min on ice. The activity of the
556 purified *C. glutamicum* (*C.g.*) gyrase as well as its inhibition by Cg1978 were determined according
557 to the manufacturer´s manual of the Gyrase (HIS) Supercoiling Assay Kits (Inspiralis, Norwich,
558 UK). According to their assay conditions, the *C.g.* gyrase concentration of 200 nM resulting in
559 complete supercoiling of 0.5 µg relaxed plasmid DNA was determined as 1 U. Supercoiling
560 inhibition of *C.g.* gyrase was assayed by using 1 U of the *C.g.* gyrase with increasing
561 concentrations of Cg1978 (0.01-5.0 µM). Additionally, different concentrations of the known

562 inhibitor ciprofloxacin (10 and 50 µM) were used as positive control. The *E. coli* BL21 (DE3) cell
563 extract was further tested as a negative control since this host was used for Cg1978 protein
564 overproduction.
565 Moreover, the inhibitory effect of Cg1978 on the *M.tb* and *E.c.* gyrase were investigated according
566 to the *M. tuberculosis and E. coli* Gyrase (HIS) Supercoiling Assay Kit (Inspiralis, Norwich, UK)
567 using 1 U of the respective gyrases and the same Cg1978 concentrations as for the *C.g.* gyrase.
568
569 ***Surface Plasmon Resonance Spectroscopy (SPR)***
570 For SPR analysis, Cg1978-C-His and GyrA-N-Strep were purified as described above. After
571 purification, the buffer of both proteins was exchanged to PBS (137 mM NaCl, 2.7 mM KCl, 8 mM
572 Na_2HPO_4, 1.5 mM KH_2PO_4, pH 7.4) using PD10 Desalting columns (GE Healthcare, Illinois, U.S).
573 Binding of His-tagged Cg1978-C-His to GyrA-N-Strep was analyzed by SPR analysis in a Biacore
574 3000 device (GE Healthcare, Freiburg, Germany) using a Sensor Chip CM5 (GE Healthcare,
575 Freiburg, Germany). As first step, an anti-histidine antibody (GE Healthcare, Freiburg, Germany)
576 was immobilized to the chip matrix using amino coupling chemistry. All experiments were carried
577 out in HBS-EP buffer (0.01 M HEPES, pH 7.4, 0.15M NaCl, 3 mM EDTA, 0.005% v/v Surfactant
578 P20) at 25°C. Following the standard coupling protocol for antibody immobilization the mixture of
579 0.05 M N-Hydroxysuccinimide (NHS) and 0.2 M 1-Ethyl-3-(3-dimethylaminopropyl) carbodiimide
580 hydrochloride (EDC) was injected for a total contact time of 420 s to activate the matrix. Then, the
581 anti-histidine antibody (50 µg ml^{-1}) diluted in immobilization buffer (10 mM sodium acetate, pH 4.5)
582 was injected for 420 s. To deactivate the unbound parts of the chip matrix, 1 M ethanolamine
583 hydrochloride-NaOH (pH 8.5) was injected for 420 s. The flow rate was set to 10 µl min^{-1} during
584 this immobilization procedure. Approximately 8.000-10.000 response units (RU) of the anti-
585 histidine antibody were immobilized per flow cell. For the binding analysis, 180-250 RU of Cg1978-
586 C-His was captured via injection of 40 µl (10 nM) at a flow rate of 5 µl min^{-1} followed by 10 min of
587 HBS-EP buffer to remove unbound protein from the chip. The binding analysis between Cg1978-

588 C-His and GyrA-N-Strep was then performed by injecting 90 µl of GyrA-N-Strep (10-250 nM)
589 followed by a dissociation time of 300 s at a flow rate of 30 µl min^{-1}. After each cycle, the surface
590 was regenerated by injection of regeneration buffer (10 mM Glycine-HCl, pH 1.5) for 30 s, at a
591 flow rate of 30 µl min^{-1}. After the equilibration with three start up cycles without the analyte, this
592 was repeated for various concentrations of GyrA-N-Strep (10 nM-250 nM). Sensorgrams were
593 recorded using Biacore 3000 Control Software 4.1.2 and analyzed with BIAevaluation software
594 4.1.1 (GE Healthcare, Freiburg, Germany). The surface of flow cell 1 immobilized with the anti-
595 histidine antibody was used to obtain blank sensorgrams for subtraction of the bulk refractive index
596 background. The referenced sensorgrams were normalized to a baseline of 0. Peaks in the
597 sensorgrams at the beginning and the end of the injection are due to the run-time difference
598 between the flow cells for the chip.

599 **Acknowledgments**

600 We thank the European Research Council (ERC Starting Grant, grant number 757563) and the
601 Helmholtz Association (grant number W2/W3-096) for financial support.
602 We thank Astrid Wirtz for technical assistance with respect to the LC-MS/MS measurement.
603 SPR analyses were performed in the Bioanalytics service unit of the JGU Biocenter.

604 **Conflict of interest**

605 The authors declare no conflict of interest.

606 **Author contributions**

607 LK, MH and JF conceived the study; LK and JB performed the experiments; LK, MH, JB, RH
608 and JF analyzed the data; LK and JF wrote the manuscript. All authors reviewed and edited
609 the manuscript.

610 **Graphical abstract**

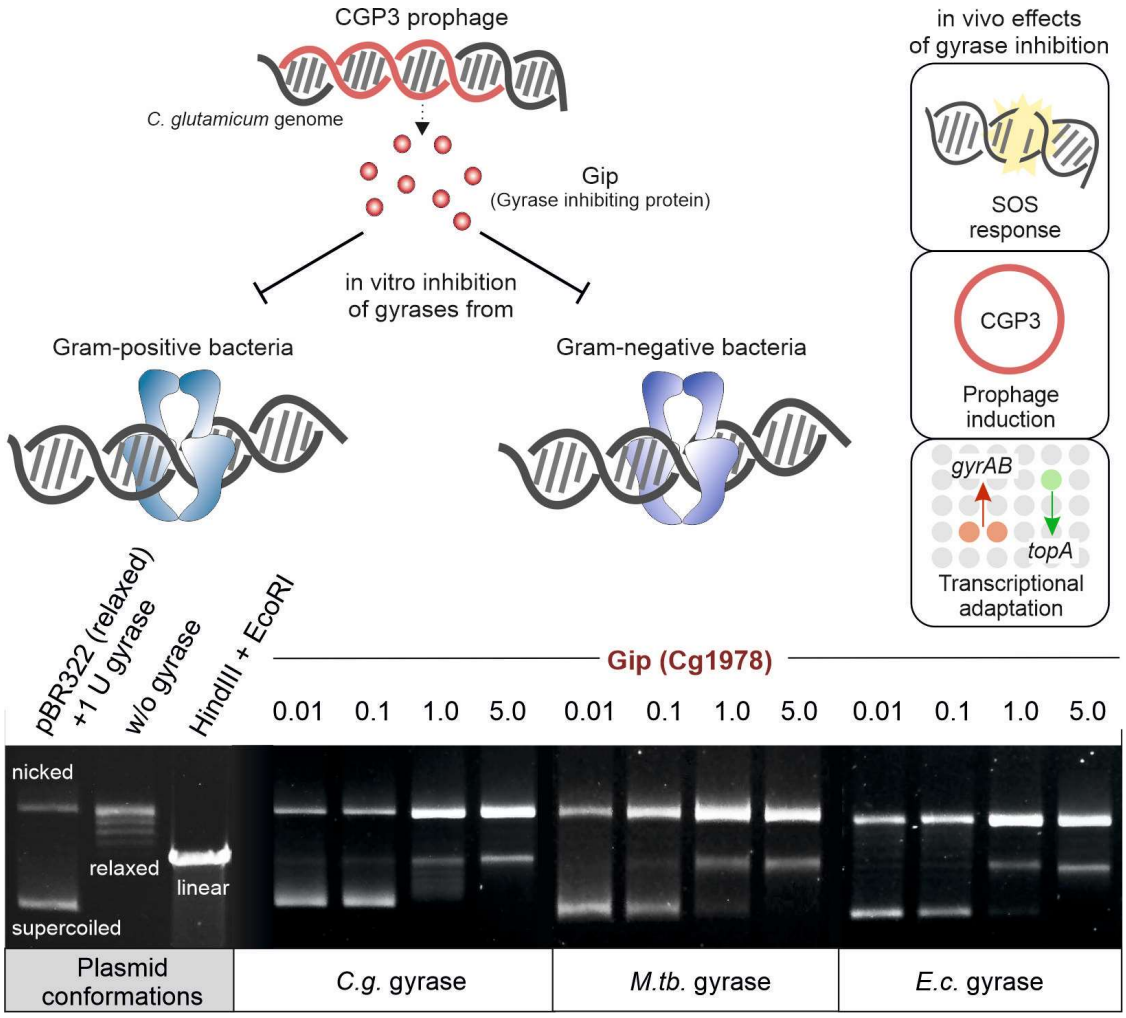

611

612 **References**

613 Ahmed, W., Menon, S., Karthik, P. V., & Nagaraja, V. (2016). Autoregulation of topoisomerase I
614 expression by supercoiling sensitive transcription. *Nucleic Acids Res, 44*(4), 1541-1552.
615 Retrieved from https://www.ncbi.nlm.nih.gov/pubmed/26496944.
616 doi:10.1093/nar/gkv1088
617 Bernard, P., Kézdy, K. E., Van Melderen, L., Steyaert, J., Wyns, L., Pato, M. L., Higgins, P. N., &
618 Couturier, M. (1993). The F Plasmid CcdB Protein Induces Efficient ATP-dependent DNA
619 Cleavage by Gyrase. *Journal of Molecular Biology, 234*(3), 534-541.
620 doi:10.1006/jmbi.1993.1609
621 Bradford, M. M. (1976). A Rapid and Sensitive Method for the Quantitation Microgram Quantities
622 of Protein Utilizing the Principle of Protein-Dye Binding. *Analytical Biochemistry, 72*, 248-
623 254. doi:10.1006/abio.1976.9999
624 Bush, N. G., Evans-Roberts, K., & Maxwell, A. (2015). DNA Topoisomerases. *EcoSal Plus, 6*(2).
625 doi:10.1128/ecosalplus.ESP-0010-2014
626 Bussmann, M., Baumgart, M., & Bott, M. (2010). RosR (Cg1324), a hydrogen peroxide-sensitive
627 MarR-type transcriptional regulator of Corynebacterium glutamicum. *J Biol Chem, 285*(38),
628 29305-29318. Retrieved from https://www.ncbi.nlm.nih.gov/pubmed/20643656.
629 doi:10.1074/jbc.M110.156372
630 Chatterji, M., Unniraman, S., Mahadevan, S., & Nagaraj, V. (2001). Effect of different classes of
631 inhibitors on DNA gyrase from Mycobacterium smegmatis. *Journal of Antimicrobial*
632 *Chemotherapy, 48*, 479–485. doi:10.1093/jac/48.4.479
633 Cheung, K. J., Badarinarayana, V., Selinger, D. W., Janse, D., & Church, G. M. (2003). A
634 microarray-based antibiotic screen identifies a regulatory role for supercoiling in the
635 osmotic stress response of Escherichia coli. *Genome Res, 13*(2), 206-215. Retrieved from
636 https://www.ncbi.nlm.nih.gov/pubmed/12566398. doi:10.1101/gr.401003
637 Collin, F., Karkare, S., & Maxwell, A. (2011). Exploiting bacterial DNA gyrase as a drug target:
638 current state and perspectives. *Appl Microbiol Biotechnol, 92*(3), 479-497. Retrieved from
639 https://www.ncbi.nlm.nih.gov/pubmed/21904817. doi:10.1007/s00253-011-3557-z
640 Dao-Thi, M. H., Van Melderen, L., De Genst, E., Afif, H., Buts, L., Wyns, L., & Loris, R. (2005).
641 Molecular basis of gyrase poisoning by the addiction toxin CcdB. *J Mol Biol, 348*(5), 1091-
642 1102. doi:10.1016/j.jmb.2005.03.049
643 De Smet, J., Hendrix, H., Blasdel, B. G., Danis-Wlodarczyk, K., & Lavigne, R. (2017).
644 Pseudomonas predators: understanding and exploiting phage-host interactions. *Nat Rev*
645 *Microbiol, 15*(9), 517-530. doi:10.1038/nrmicro.2017.61
646 DeMarini, D. M., & Lawrence, B. K. (1992). Prophage induction by DNA topoisomerase II poisons
647 and reactive-oxygen species: Role of DNA breaks. *Mutation Research, 267*, 1-17.
648 doi:10.1016/0027-5107(92)90106-C
649 Ding, Y., Manzo, C., Fulcrand, G., Leng, F., Dunlap, D., & Finzi, L. (2014). DNA supercoiling: a
650 regulatory signal for the lambda repressor. *Proc Natl Acad Sci U S A, 111*(43), 15402-
651 15407. Retrieved from https://www.ncbi.nlm.nih.gov/pubmed/25319264.
652 doi:10.1073/pnas.1320644111
653 Donovan, C., Heyer, A., Pfeifer, E., Polen, T., Wittmann, A., Kramer, R., Frunzke, J., & Bramkamp,
654 M. (2015). A prophage-encoded actin-like protein required for efficient viral DNA replication
655 in bacteria. *Nucleic Acids Res, 43*(10), 5002-5016. Retrieved from
656 https://www.ncbi.nlm.nih.gov/pubmed/25916847. doi:10.1093/nar/gkv374
657 Dorman, C. J., & Dorman, M. J. (2016). DNA supercoiling is a fundamental regulatory principle in
658 the control of bacterial gene expression. *Biophys Rev, 8*(3), 209-220. Retrieved from
659 https://www.ncbi.nlm.nih.gov/pubmed/28510224. doi:10.1007/s12551-016-0205-y
660 Drlica, K., & Malik, M. (2003). Fluoroquinolones: Action and Resistance. *Current Topics in*
661 *Medicinal Chemistry, 3*(249), 249-282. doi:10.2174/1568026033452537

662 Dwyer, D. J., Kohanski, M. A., Hayete, B., & Collins, J. J. (2007). Gyrase inhibitors induce an
663 oxidative damage cellular death pathway in Escherichia coli. *Mol Syst Biol, 3*(91).
664 Retrieved from https://www.ncbi.nlm.nih.gov/pubmed/17353933.
665 doi:10.1038/msb4100135
666 Falzon, D., Gandhi, N., Migliori, G. B., Sotgiu, G., Cox, H. S., Holtz, T. H., Hollm-Delgado, M. G.,
667 Keshavjee, S., DeRiemer, K., Centis, R., D'Ambrosio, L., Lange, C. G., Bauer, M., &
668 Menzies, D. (2013). Resistance to fluoroquinolones and second-line injectable drugs:
669 impact on multidrug-resistant TB outcomes. *Eur Respir J, 42*(1), 156-168. Retrieved from
670 https://www.ncbi.nlm.nih.gov/pubmed/23100499. doi:10.1183/09031936.00134712
671 Frunzke, J., Bramkamp, M., Schweitzer, J. E., & Bott, M. (2008). Population Heterogeneity in
672 *Corynebacterium glutamicum* ATCC 13032 caused by prophage CGP3. *Journal of*
673 *Bacteriology, 190*(14), 5111-5119. Retrieved from
674 http://www.ncbi.nlm.nih.gov/pubmed/18487330. doi:10.1128/JB.00310-08
675 Gibson, D. G. (2011). Enzymatic assembly of overlapping DNA fragments. *Methods Enzymology,*
676 *498*, 349-361. Retrieved from https://www.ncbi.nlm.nih.gov/pubmed/21601685.
677 doi:10.1016/B978-0-12-385120-8.00015-2
678 Grünberger, A., Probst, C., Helfrich, S., Nanda, A., Stute, B., Wiechert, W., von Lieres, E., Noh,
679 K., Frunzke, J., & Kohlheyer, D. (2015). Spatiotemporal microbial single-cell analysis using
680 a high-throughput microfluidics cultivation platform. *Cytometry A, 87*(12), 1101-1115.
681 Retrieved from https://www.ncbi.nlm.nih.gov/pubmed/26348020.
682 doi:10.1002/cyto.a.22779
683 Grünberger, A., van Ooyen, J., Paczia, N., Rohe, P., Schiendzielorz, G., Eggeling, L., Wiechert,
684 W., Kohlheyer, D., & Noack, S. (2013). Beyond growth rate 0.6: Corynebacterium
685 glutamicum cultivated in highly diluted environments. *Biotechnol Bioeng, 110*(1), 220-228.
686 Retrieved from https://www.ncbi.nlm.nih.gov/pubmed/22890752. doi:10.1002/bit.24616
687 Guha, S., Udupa, S., Ahmed, W., & Nagaraja, V. (2018). Rewired Downregulation of DNA Gyrase
688 Impacts Cell Division, Expression of Topology Modulators, and Transcription in
689 Mycobacterium smegmatis. *J Mol Biol, 430*(24), 4986-5001. Retrieved from
690 https://www.ncbi.nlm.nih.gov/pubmed/30316784. doi:10.1016/j.jmb.2018.10.001
691 Hatfull, G. F. (2015). Dark Matter of the Biosphere: the Amazing World of Bacteriophage Diversity.
692 *J Virol, 89*(16), 8107-8110. doi:10.1128/jvi.01340-15
693 Helfrich, S., Pfeifer, E., Kramer, C., Sachs, C. C., Wiechert, W., Kohlheyer, D., Noh, K., & Frunzke,
694 J. (2015). Live cell imaging of SOS and prophage dynamics in isogenic bacterial
695 populations. *Mol Microbiol, 98*(4), 636-650. Retrieved from
696 https://www.ncbi.nlm.nih.gov/pubmed/26235130. doi:10.1111/mmi.13147
697 Heyer, A., Gatgens, C., Hentschel, E., Kalinowski, J., Bott, M., & Frunzke, J. (2012). The two-
698 component system ChrSA is crucial for haem tolerance and interferes with HrrSA in haem-
699 dependent gene regulation in Corynebacterium glutamicum. *Microbiology, 158*, 3020-
700 3031. Retrieved from https://www.ncbi.nlm.nih.gov/pubmed/23038807.
701 doi:10.1099/mic.0.062638-0
702 Ikeda, M., & Nakagawa, S. (2003). The Corynebacterium glutamicum genome: features and
703 impacts on biotechnological processes. *Appl Microbiol Biotechnol, 62*(2-3), 99-109.
704 Retrieved from https://www.ncbi.nlm.nih.gov/pubmed/12743753. doi:10.1007/s00253-
705 003-1328-1
706 Janion, C. (2008). Inducible SOS response system of DNA repair and mutagenesis in Escherichia
707 coli. *International Journal of Biological Sciences, 4*(6), 338-344. doi:10.7150/ijbs.4.338
708 Jeong, K. S., Xie, Y., Hiasa, H., & Khodursky, A. B. (2006). Analysis of pleiotropic transcriptional
709 profiles: a case study of DNA gyrase inhibition. *PLoS Genet, 2*(9), e152. Retrieved from
710 https://www.ncbi.nlm.nih.gov/pubmed/17009874. doi:10.1371/journal.pgen.0020152
711 Kensy, F., Zang, E., Faulhammer, C., Tan, R. K., & Buchs, J. (2009). Validation of a high-
712 throughput fermentation system based on online monitoring of biomass and fluorescence

713 in continuously shaken microtiter plates. *Microb Cell Fact, 8*(31). Retrieved from
714 https://www.ncbi.nlm.nih.gov/pubmed/19497126. doi:10.1186/1475-2859-8-31
715 Laemmli, U. K. (1970). Cleavage of Structural Proteins during Assembly of Head of Bacteriophage
716 T4. *Nature, 227*, 680-685. doi:10.1038/227680a0
717 Madhusudan, K., & Nagaraja, V. (1996). Alignment and phylogenetic analysis of type II DNA
718 topoisomerases. *Journal of Biosciences, 21*, 613-629. doi:10.1007/BF02703140
719 Manjunatha, U. H., Dalal, M., Chatterji, M., Radha, D. R., Visweswariah, S. S., & Nagaraja, V.
720 (2002). Functional characterisation of mycobacterial DNA gyrase: an efficient decatenase.
721 *Nucleic Acids Res, 30*(10), 2144–2153. doi:10.1093/nar/30.10.2144
722 Manjunatha, U. H., Madhusudan, K., Visweswariah, S., & Nagaraja, V. (2000). Structural
723 heterogeneity in DNA gyrases in Gram-positive and Gram-negative bacteria. *Current*
724 *Science, 79*(7), 968-974.
725 Massé, E., & Drolet, M. (1999). Relaxation of Transcription-induced Negative Supercoiling Is an
726 Essential Function of Escherichia coli DNA Topoisomerase I. *Journal of Biological*
727 *Chemistry, 274*(23), 16654–16658. doi:10.1074/jbc.274.23.16654
728 Mattenberger, Y., Silva, F., & Belin, D. (2015). 55.2, a phage T4 ORFan gene, encodes an inhibitor
729 of Escherichia coli topoisomerase I and increases phage fitness. *PLoS One, 10*(4),
730 e0124309. Retrieved from https://www.ncbi.nlm.nih.gov/pubmed/25875362.
731 doi:10.1371/journal.pone.0124309
732 Maxwell, A., & Lawson, D. M. (2003). The ATP-Binding Site of Type II Topoisomerases as a Target
733 for Antibacterial Drugs. *Current Topics in Medicinal Chemistry, 3*(3), 283-303.
734 doi:10.2174/1568026033452500
735 Menzel, R., & Gellert, M. (1983). Regulation of the Genes for E. coli DNA Gyrase: Homeostatic
736 Control of DNA Supercoiling. *Cell, 34*, 105-113. doi:10.1016/0092-8674(83)90140-X
737 Miki, T., Park, J. A., Nagao, K., Murayama, N., & Horiuchi, T. (1992). Control of segregation of
738 chromosomal DNA by sex factor F in Escherichia coli. Mutants of DNA gyrase subunit A
739 suppress letD (ccdB) product growth inhibition. *J Mol Biol, 225*(1), 39-52.
740 doi:10.1016/0022-2836(92)91024-j
741 Nanda, A. M., Heyer, A., Kramer, C., Grunberger, A., Kohlheyer, D., & Frunzke, J. (2014). Analysis
742 of SOS-induced spontaneous prophage induction in Corynebacterium glutamicum at the
743 single-cell level. *J Bacteriol, 196*(1), 180-188. Retrieved from
744 https://www.ncbi.nlm.nih.gov/pubmed/24163339. doi:10.1128/JB.01018-13
745 Niebisch, A., & Bott, M. (2001). Molecular analysis of the cytochrome bc1-aa3 branch of the
746 Corynebacterium glutamicum respiratory chain containing an unusual diheme cytochrome
747 c1. *Arch Microbiol, 175*(4), 282-294. Retrieved from
748 https://www.ncbi.nlm.nih.gov/pubmed/11382224. doi:10.1007/s002030100262
749 Nobrega, F. L., Vlot, M., de Jonge, P. A., Dreesens, L. L., Beaumont, H. J. E., Lavigne, R., Dutilh,
750 B. E., & Brouns, S. J. J. (2018). Targeting mechanisms of tailed bacteriophages. *Nat Rev*
751 *Microbiol, 16*(12), 760-773. doi:10.1038/s41579-018-0070-8
752 Norregaard, K., Andersson, M., Sneppen, K., Nielsen, P. E., Brown, S., & Oddershede, L. B.
753 (2013). DNA supercoiling enhances cooperativity and efficiency of an epigenetic switch.
754 *Proc Natl Acad Sci U S A, 110*(43), 17386-17391. Retrieved from
755 https://www.ncbi.nlm.nih.gov/pubmed/24101469. doi:10.1073/pnas.1215907110
756 Norregaard, K., Andersson, M., Sneppen, K., Nielsen, P. E., Brown, S., & Oddershede, L. B.
757 (2014). Effect of supercoiling on the lambda switch. *Bacteriophage, 4*(1), e27517.
758 Retrieved from https://www.ncbi.nlm.nih.gov/pubmed/24386605. doi:10.4161/bact.27517
759 Ofir, G., & Sorek, R. (2018). Contemporary Phage Biology: From Classic Models to New Insights.
760 *Cell, 172*(6), 1260-1270. Retrieved from
761 https://www.sciencedirect.com/science/article/pii/S0092867417313053?via%3Dihub.
762 doi:10.1016/j.cell.2017.10.045

763 Orr, M. W., Mao, Y., Storz, G., & Qian, S. B. (2020). Alternative ORFs and small ORFs: shedding
764 light on the dark proteome. *Nucleic Acids Res, 48*(3), 1029-1042. Retrieved from
765 https://www.ncbi.nlm.nih.gov/pubmed/31504789. doi:10.1093/nar/gkz734
766 Pfeifer, E., Hunnefeld, M., Popa, O., Polen, T., Kohlheyer, D., Baumgart, M., & Frunzke, J. (2016).
767 Silencing of cryptic prophages in Corynebacterium glutamicum. *Nucleic Acids Res, 44*(21),
768 10117-10131. Retrieved from https://www.ncbi.nlm.nih.gov/pubmed/27492287.
769 doi:10.1093/nar/gkw692
770 Pierrat, O. A., & Maxwell, A. (2003). The action of the bacterial toxin microcin B17. *J Biol Chem,*
771 *278*(37), 35016-35023. Retrieved from https://www.ncbi.nlm.nih.gov/pubmed/12829716.
772 doi:10.1074/jbc.M304516200
773 Polen, T., & Wendisch, V. F. (2004). Genomewide expression analysis in amino acid-producing
774 bacteria using DNA microarrays.pdf>. *Applied Biochemistry and Biotechnology, 118*, 215-
775 232. doi:0.1385/ABAB:118:1-3:215
776 Reece, R. J., & Maxwell, A. (1991). DNA gyrase: structure and function. *Crit Rev Biochem Mol*
777 *Biol, 26*(3-4), 335-375. Retrieved from https://www.ncbi.nlm.nih.gov/pubmed/1657531.
778 doi:10.3109/10409239109114072
779 Roach, D. R., & Donovan, D. M. (2015). Antimicrobial bacteriophage-derived proteins and
780 therapeutic applications. *Bacteriophage, 5*(3), e1062590. Retrieved from
781 https://www.ncbi.nlm.nih.gov/pubmed/26442196. doi:10.1080/21597081.2015.1062590
782 Rohwer, F., & Youle, M. (2011). Consider something viral in your search. *Nat Rev Microbiol, 9*(5),
783 308-309. doi:10.1038/nrmicro2563
784 Sambrook, J., & Russell, D. W. (2001). *Molecular Cloning: A Laboratory Manual*: Cold Spring
785 Harbor Laboratory Press, NY.
786 Schroven, K., Aertsen, A., & Lavigne, R. (2021). Bacteriophages as drivers of bacterial virulence
787 and their potential for biotechnological exploitation. *FEMS Microbiol Rev, 45*(1), 1–15.
788 Retrieved from https://www.ncbi.nlm.nih.gov/pubmed/32897318.
789 doi:10.1093/femsre/fuaa041
790 Sivaraman, T., Kumar, T. K. S., Jayaraman, G., & Yu, C. (1997). The Mechanism of 2,2,2-
791 Trichloroacetic Acid-Induced Protein Precipitation. *Journal of Protein Chemistry, 16*(4),
792 291–297. doi:10.1023/A:1026357009886
793 Storz, G., Wolf, Y. I., & Ramamurthi, K. S. (2014). Small proteins can no longer be ignored. *Annu*
794 *Rev Biochem, 83*, 753-777. Retrieved from
795 https://www.ncbi.nlm.nih.gov/pubmed/24606146. doi:10.1146/annurev-biochem-070611-
796 102400
797 Tomasz, M. (1995). Mitomycin C: small, fast and deadly (but very selective). *Chemistry & Biology,*
798 *2*(9), 575-579. doi:10.1016/1074-5521(95)90120-5
799 Vanden Broeck, A., Lotz, C., Ortiz, J., & Lamour, V. (2019). Cryo-EM structure of the complete *E.*
800 *coli* DNA gyrase nucleoprotein complex. *Nat Commun, 10*(1), 4935. doi:10.1038/s41467-
801 019-12914-y
802 Wendisch, V. F., Jorge, J. M. P., Perez-Garcia, F., & Sgobba, E. (2016). Updates on industrial
803 production of amino acids using Corynebacterium glutamicum. *World J Microbiol*
804 *Biotechnol, 32*(6), 105. Retrieved from https://www.ncbi.nlm.nih.gov/pubmed/27116971.
805 doi:10.1007/s11274-016-2060-1
806 Wiechert, J., Filipchyk, A., Hünnefeld, M., Gätgens, C., Brehm, J., Heermann, R., & Frunzke, J.
807 (2020). Deciphering the Rules Underlying Xenogeneic Silencing and Counter-Silencing of
808 Lsr2-like Proteins Using CgpS of *Corynebacterium glutamicum* as a Model. *mBio, 11*(1),
809 e02273-02219. doi:10.1128/mBio.02273-19
810 Yin, Y., & Fischer, D. (2008). Identification and investigation of ORFans in the viral world. *BMC*
811 *Genomics, 9*(24). Retrieved from https://www.ncbi.nlm.nih.gov/pubmed/18205946.
812 doi:10.1186/1471-2164-9-24
813

814 **Supplementary Information**

815

816 **Table S1:** Bacterial strains used in this study.

817 **Table S2:** Plasmids used in this study.

818 **Table S3:** Oligonucleotides used in this study.

819 **Table S4:** Impact of cg1978 overexpression on global expression levels.

820

821 **Figure S1:** Screening of small phagic proteins regarding their impact on cellular growth and CGP3

822 induction in *C. glutamicum.*

823 **Figure S2:** Cell growth and prophage inducibility in the Δcg1914 or Δcg1978 mutant strain.

824 **Figure S3:** Purification of proteins for surface plasmon resonance spectroscopy of protein-protein

825 interaction.

826 **Figure S4:** Sequence alignment of the DNA gyrase subunit from *C. glutamicum* (C),

827 *M. tuberculosis* (M) and *E. coli* (E).

828 **Figure S5:** Sequence alignment of the DNA gyrase subunit B from *C. glutamicum* (C),

829 *M. tuberculosis* (M) and *E. coli* (E).

830 **Figure S6:** Gyrase activity assay.

831 **Figure S7**: Cell growth of *E. coli* BL21 (DE3) under gip overexpression conditions

832

833 **Video S1:** Time lapse video of a *C. glutamicum* microcolony of the prophage reporter strain under

834 cg1978 overexpression (50 µM IPTG).

835 **Video S2:** Time lapse video of a *C. glutamicum* microcolony of the prophage reporter strain under

836 standard conditions (0 µM IPTG).